ACS OMEGA

Open Access

http://pubs.acs.org/journal/acsodf

Article

Epidermal Sensors Constructed by a Stabilized Nanosilver Hydrogel with Self-Healing, Antimicrobial, and Temperature-Responsive Properties

Xiongbiao Zheng, Jiachang Chen, and Xia Huang*

Cite This: *ACS Omega* 2024, 9, 49001−49012

Read Online

ACCESS | Metrics & More | Article Recommendations | Supporting Information

ABSTRACT: The development of conductive hydrogels has garnered significant attention in the field of wearable devices and smart sensors. However, the fabrication of hydrogels that possess both multifunctionality and structural stability remains a challenging task. In this study, a novel hydrogel, P_{Ag}HCB, was synthesized using a mild method and exhibited outstanding characteristics such as electrical conductivity, self-healing capability, antimicrobial activity, dimensional stability, and temperature sensitivity. The exceptional mechanical performance (∼120 kPa at a strain of 450%) of P_{Ag}HCB is attributed to the incorporation of hydroxypropylmethylcellulose (HPMC) and the mechanical reinforcement of the gel network by carboxylated carbon nanotubes (CNT-COOH). The borate bonds between or within poly(vinyl alcohol) (PVA) chains confer self-healing capabilities upon P_{Ag}HCB, with a healing efficiency of 74.1%. The in situ reduction of silver nanoparticles through ultraviolet irradiation imparts antimicrobial characteristics to the hydrogel [against *Escherichia coli*, zone of inhibition (ZOI) = 3.7 mm; against *Staphylococcus aureus*, ZOI = 6.3 mm]. The linear temperature responsiveness of the P_{Ag}HCB hydrogel ($R = -3.99T + 608.84$ and COD = 0.9988) arises from the migration of silver ions within the gel matrix and the dissociation of borate bonds. Furthermore, P_{Ag}HCB was seamlessly integrated into sensors designed for monitoring human motion. The gel-based sensors exhibited three distinct sensing strain ranges corresponding to three different gauge factors (GF_1 = 2.976, GF_2 = 1.063, and GF_3 = 2.97). Notably, P_{Ag}HCB gel sensors demonstrated the capability to detect electrical signals generated by finger and wrist joint movements and even discerned signals arising from subtle deformations induced by activities such as speaking. Additionally, the P_{Ag}HCB gel was utilized as a pressure sensor to detect external pressures applied to the skin (from 0.373 to 15.776 kPa). This work expands the avenues for designing and synthesizing multifunctional conductive hydrogels, promoting the application of hydrogel sensors with comfortable wear and high sensitivity.

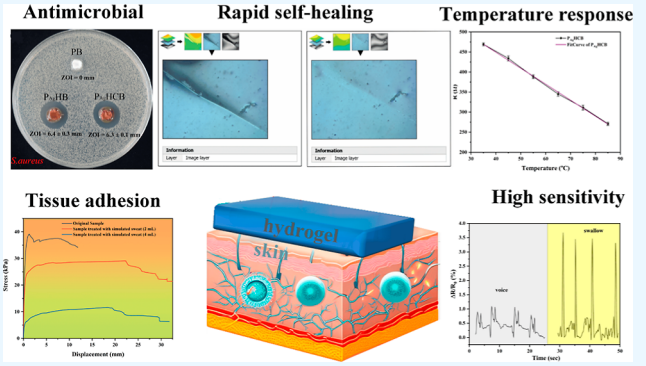

INTRODUCTION

In recent years, there has been a growing interest in the utilization of conductive hydrogels within the domains of wearable technology, electronic skin, and biosignal monitoring owing to their commendable biocompatibility and adjustable mechanical characteristics.[1−6] Typically, employing flexible polymers as substrates and conductive fillers as the conductive medium, these hydrogels encompass a range of materials, including conductive polymers,[7] metal-based nanomaterials,[8] carbon-based materials,[9] MXene,[10] and liquid metals.[11] Nonorganic conductive materials, especially metal-based nanomaterials, have garnered substantial attention from researchers due to their heightened specific surface area, facile modification, and straightforward synthesis.[12] Beyond their conductive properties, gel sensors necessitate additional attributes, such as self-healing capabilities derived from dynamic covalent bonding and noncovalent cross-linking.[13] Dynamic covalent bonds encompass imine, hydrazide, disulfide, borate, and Diels−Alder reactions. Noncovalent bonds include host−guest interactions, ionic bonds, and hydrogen bonds. Borate bonds, formed by boric acid interacting with diols, are intriguing due to their easy preparation, quick self-healing, and high efficiency in promoting healing. A recent study by Zhao et al. has successfully engineered a self-healing hydrogel based on poly(vinyl alcohol) (PVA), sodium alginate, and tannic acid, demonstrating commendable tensile properties, plasticity, rapid self-healing and sensing capabilities.[14]

Received: December 18, 2023
Revised: February 26, 2024
Accepted: March 1, 2024
Published: December 2, 2024

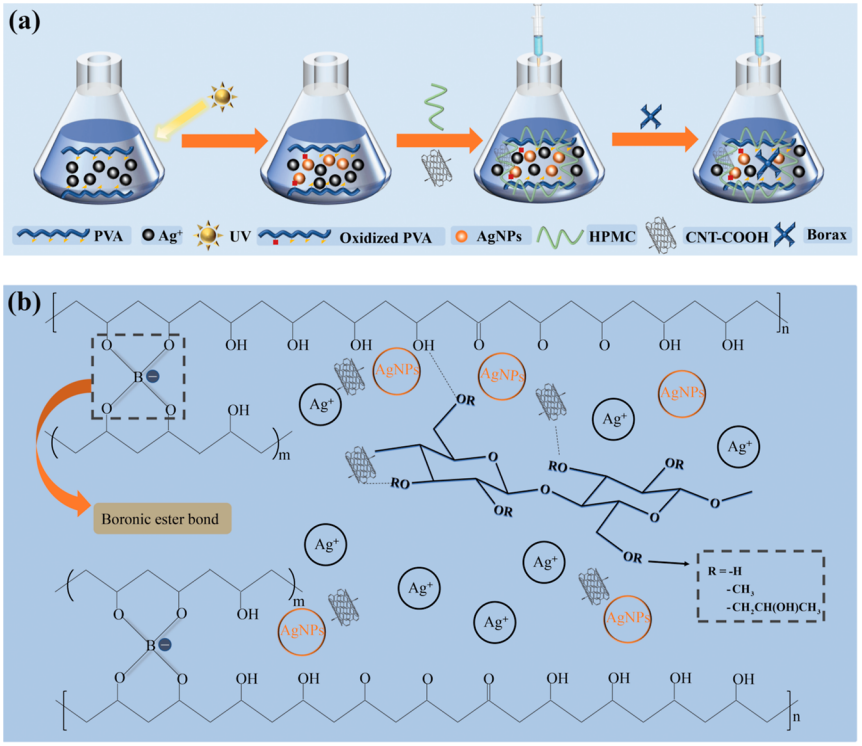

Figure 1. (a) Preparation process of the P_{Ag}HCB hydrogel. (b) Dynamic covalent cross-linking (borate ester bonds) and physical cross-linking (hydrogen bonds and electrostatic interaction) in the P_{Ag}HCB hydrogel network based on PVA, HPMC, AgNPs, and borax.

Poly(vinyl alcohol) (PVA) is a chemically stable, biocompatible, and cost-effective polymer, making it a preferred choice for the fabrication of composite membranes and hydrogel composites. In the realm of metal nanoparticle synthesis, PVA serves the dual role of a reducing agent and stabilizer, adding to its versatility. Moreover, the crystallinity of PVA within hydrogels can be manipulated through a freeze−thaw process, enhancing mechanical properties and allowing for the tailored design of hydrogels with varying strengths and compositions.[15] More importantly, poly(vinyl alcohol) can react with borax to form dynamic covalent bonds known as borate ester bonds.[16]

Addressing the biofouling challenge encountered by wearable devices, particularly the accumulation of microorganisms and metabolites on the skin interface, silver nanoparticles (AgNPs) present a promising solution owing to their antimicrobial and conductive attributes.[17] Taesuwan[18] and colleagues have reported the preparation of hydrogels incorporating AgNPs synthesized from sugarcane leaves, showcasing the potential of AgNPs in mitigating biofouling. However, challenges such as agglomeration and oxidation often arise with silver nanoparticles in gel systems. Hydroxypropylmethylcellulose (HPMC), a water-soluble polymer, offers versatility as a slow-release agent, thickener, and adhesive, exhibiting good biocompatibility, high stability, adjustable slow-release properties, and negligible toxic side effects.[19] Incorporating HPMC into hydrogels not only improves their mechanical properties but also enhances the stability of nanosilver, attributed to its charge stability, adsorption, and spatial site resistance effects. Generally speaking, hydrogels containing nanosilver may experience aggregation or oxidation of the internal nanosilver over prolonged periods of static conditions or exposure to external stimuli, thereby affecting the conductivity of the hydrogel. Through the encapsulation effect of hydroxypropyl methylcellulose (HPMC), the numerous hydroxyl groups on the molecular chains can prevent nanosilver from undergoing denaturation. Carboxylation of carbon nanotubes enhances their interaction with hydrogels, leading to a significant improvement in mechanical properties and stability when employed as carbon enhancers.[20] Furthermore, the addition of carboxylated carbon nanotubes enhances hydrogel adhesion, boosting the tensile and compressive strength. Therefore, significant progress is anticipated in the development of customized conductive, antimicrobial, and self-healing hydrogels for physiological signal monitoring and sensing applications through the use of the aforementioned materials.

Considering the mechanical, antimicrobial, and conductive requisites of hydrogel sensors, this study introduces a composite hydrogel synthesized by incorporating hydroxypropylmethylcellulose (HPMC) and carboxylated carbon nanotubes into an irradiation-reduced PVA/nanosilver solution. Controlled by a micropump to modulate the flow rate of sodium tetraborate solution, a gradual cross-linking process was employed in the preparation. The composite hydrogel is predominantly structured through dynamic borate bonds (formed between PVA chains containing *cis*-diols and the cross-linker borax) and multiple hydrogen bonds (interactions among PVA, HPMC, and CNT-COOH). The resultant hydrogels demonstrate exceptional mechanical strength, electrical conductivity, prompt self-healing attributes, antimicrobial efficacy, and linear temperature response characteristics. Remarkably, the hydrogel exhibits impressive tensile properties (tensile strain, ∼450%), effective self-healing (HE = 74.1%), conductivity, antimicrobial features, and enhanced sensitivity. As a result, the hydrogel serves as a versatile strain sensor, capable of monitoring a wide range of human movements, including detailed actions such as finger and wrist motions as well as subtle activities such as swallowing and

https://doi.org/10.1021/acsomega.3c10135
ACS Omega 2024, 9, 49001−49012

speaking. Additionally, it functions adeptly as a pressure sensor, proficient in detecting external pressures on the skin.

EXPERIMENTAL SECTION

Experimental Materials. The materials used are poly(vinyl alcohol) (PVA, type 1799), silver nitrate solution (0.1 M), hydroxypropylmethylcellulose (HPMC), sodium tetraborate (99%), carboxylated carbon nanotubes (CNT-COOH, >98%, OD: 30−50 nm, and length: <10 μm), rhodamine 6G (95%), methyl blue (AR), and Vaseline (medical grade). All the above reagents were purchased from Shanghai Aladdin Biochemical Technology Co.

Preparation of the P_{Ag}HCB Hydrogel. In order to harmonize self-healing ability, electrical conductivity, and antimicrobial properties in a hydrogel system, we designed a process (Figure 1a). The poly(vinyl alcohol)/nanosilver solution was first reduced using UV irradiation at a specific wavelength (365 nm), and a certain amount of aqueous hydroxypropylmethylcellulose (1 wt %) was added with vigorous stirring until it was well-mixed, followed by injection of CNT-COOH dispersed in deionized water into the polymer solution via a micropump (50 μL/min) and stirring until well dispersed. Sodium tetraborate solution was then added to the reaction system by micropumping (100 μL/min) and stirred for half an hour in a water bath at 50 °C. After the reaction, the composite hydrogel, P_{Ag}HCB, was formed by standing for 30 min. For the control experiments, hydrogel specimens with different compositions were prepared accordingly (Table S1).

Characterization. All mechanical tests were performed by using a universal tensile tester (CMT6103) equipped with a 50 N load cell at a speed of 100 mm/min. The resistance of the specimens was measured using an CS310M electrochemical workstation (Corrtest, China). The infrared absorption curves of the hydrogels were obtained by the ATR-FTIR (Thermo Scientific Nicolet iS20) method with wave numbers ranging from 600 to 4000 cm^{-1}. Thermogravimetric analysis was performed using a TG 209 F3 Tarsus (NETZSCH, Germany) instrument with the samples heated from 25 to 600 °C in a nitrogen atmosphere at a heating rate of 10 °C/min. Scanning electron microscopy (SEM) images were provided by a field emission scanning electron microscope (Hitachi Regulus 8100). Optical images were obtained using a smartphone (Redmi K40). The size distribution of nanosilver was determined using a nanoparticle size analyzer (Malvern Zetasizer Nano ZS90).

Self-Healing Test. Prior to the self-healing test, gel specimens with fixed dimensions were prepared by using a mold (Figure S3). The original specimens were stained by rhodamine 6G and methyl blue on two identical component specimens, respectively; then, the specimens were healed by using a scalpel to cut the specimens transversely of the cross sections of different colors in contact with each other for a period of time. The healing efficiency was calculated by comparing the maximum stress values of the stress−strain curves before and after healing with the following formula

$$\mathrm{HE} = \frac{T_{\mathrm{After}}}{T_{\mathrm{Before}}} \times 100\% \quad (1)$$

where T_{After} and T_{Before} denote the fracture stresses of the healed and initial specimens in tensile testing, respectively.[21] The healing process was then observed by laser confocal microscopy, and the optical images and height distribution maps corresponding to different moments were recorded, respectively.

Temperature Responsiveness Test. To assess the temperature responsiveness of the hydrogel, it is essential to eliminate the Joule effect.[22] Applying currents of 0.1 and 10^{-5} A through an electrochemical workstation, the temperature changes on the hydrogel were observed using an infrared camera under high- and low-current conditions, respectively. The energization durations were set at 10, 20, and 30 min. To measure the change in the hydrogel's resistance with temperature, the test hydrogel was positioned on a thermostatic heating table, coated with a layer of Vaseline on its surface to prevent moisture evaporation, and connected to the electrochemical workstation. The hydrogel was kept at a constant temperature for 10 min before each electrochemical data acquisition.

Adhesion Performance Test. In order to examine the adhesion of the hydrogel on the skin surface, the porcine epidermis was used for the adhesion behavior of the hydrogel. Briefly, the P_{Ag}HCB hydrogel (20 mm × 20 mm × 1 mm) was placed between two pieces of porcine epidermis for 1 min. The two substrates were then stretched to separation on a universal material testing machine at 100 mm/min. The adhesion strength was calculated as the maximum measured tensile force (N) divided by the contact area of the sample (m^2). Furthermore, adhesion tests of the hydrogel were conducted under simulated human epidermal sweating conditions. Simulated sweat was prepared by ultrasonically mixing 20 mg of urea, 30 mg of lactic acid, 20 mg of sodium chloride, 15 mg of potassium chloride, and 15 mg of calcium chloride in 10 g of deionized water. The simulated sweat was then sprayed onto the pig epidermis, and adhesion tests were performed. The adhesion strengths before and after spraying were compared to determine compliance with the requirements for epidermal sensors.[23]

Electrical Performance Test. The electrical signals of the sensors were acquired with an electrochemical workstation. In the electrical property test, the P_{Ag}HCB hydrogel was plasticized into a certain regular shape through a prepared mold. In addition, the conductivity (σ, S/m) of the hydrogel was calculated according to the equation $\sigma = L/(R \times A)$, where L is the distance between two neighboring probes (m), R represents the resistance of the hydrogel (Ω), and A denotes the cross-sectional area (m^2). The relative resistance change was calculated according to the equation $\Delta R/R_0 = (R - R_0)/R_0$, where R_0 and R are the resistance without and with strain, respectively. During electrical testing, the voltage was set to 0.5 V.[24]

Antimicrobial Performance Test. Three bacterial culture tubes, each containing 3 mL of liquid medium, were prepared. Single colonies were picked from the solid medium of *Staphylococcus aureus* and *Escherichia coli* and added to the liquid medium in two of the tubes, while the third tube served as a blank control. The samples were incubated overnight in a temperature-controlled shaker (37 °C and 200 rpm). Subsequently, the samples were placed in centrifuge tubes according to their groups, sterilized by soaking in 75% alcohol for 30 min, and then transferred to disposable Petri dishes to air-dry before being set aside.[25] The bacterial solutions of *E. coli* and *S. aureus* were diluted to 10^6 CFU/mL with sterile PBS. A 100 μL aliquot of each diluted solution was spread evenly on a solid medium. The sterilized samples were affixed to the surface of the medium and gently pressed with sterile

https://doi.org/10.1021/acsomega.3c10135
ACS Omega 2024, 9, 49001−49012

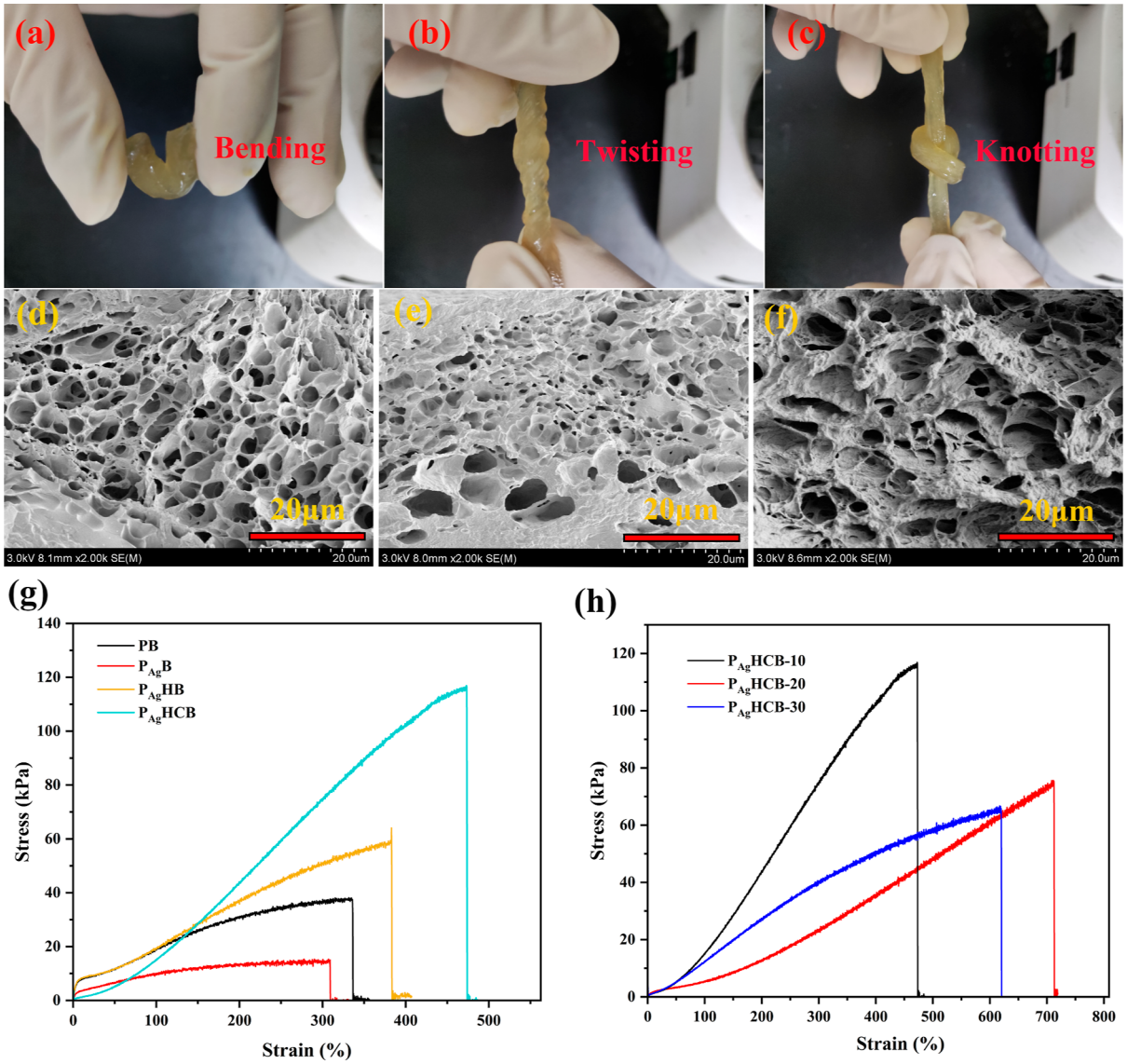

Figure 2. Images of the $P_{Ag}HB$ hydrogel in (a) bending, (b) twisting, and (c) knotting states. SEM images of cross sections of freeze-dried (d) $P_{Ag}B$, (e) $P_{Ag}HB$, and (f) $P_{Ag}HCB$ hydrogels. (g) Stress−strain curves of hydrogels of different compositions. (h) Stress−strain curves of $P_{Ag}HCB$ hydrogels with different CNT-COOH concentrations.

tweezers to ensure full contact. The Petri dishes were then incubated in a temperature-controlled incubator at 37 °C for 24 h. After incubation, the samples were removed and photographed with a camera, and the size of the zone of inhibition (ZOI) was measured and recorded.[26] The diameter of the ZOI was calculated using the formula

$$\mathrm{ZOI} = \frac{D_i - d_p}{2} \quad (2)$$

where D_i and d_p represent the average outer diameter of the ZOI (mm) and the diameter of the specimen (mm), respectively.

RESULTS AND DISCUSSION

Chemical Structure and Thermal Analysis of the Hydrogels. Infrared spectroscopy was employed to characterize the physical and chemical bonding in the hydrogel.[27] As shown in Figure S1, comparative analysis of PB and $P_{Ag}B$ samples revealed a reduction in the methylene vibrational peak at 2919 cm^{-1} and an enhancement in the carbonyl absorption peak at 1677 cm^{-1}, indicating the reduction of silver nitrate by PVA. This is attributed to changes in the chemical structure of PVA induced by the reduction reaction, including the formation of carbonyl groups and the breakage of C−H bonds in the methylene groups. Upon the addition of HPMC and CNT-COOH, the absorption peaks exhibited increased intensity and shifted to higher wavenumbers, implying enhanced carbon−hydrogen vibrations due to the interaction between PVA molecular chains and CNT-COOH. Additionally, the absorption peak at 1648 cm^{-1} corresponds to the vibrational motion of the carbon−oxygen double bond in CNT-COOH. Peaks at 1416 and 1330 cm^{-1} represent asymmetric stretching relaxation peaks of B−O−C, indicating the formation of borate bonds, while the peak at 834 cm^{-1} is likely the B−O stretching peak of residual $B(OH)_4^-$.[28] At 1082 and 1032 cm^{-1}, vibrations related to C−O−H and C−C bonds in the carbon skeleton were observed, and their intensities increased upon the addition of CNT-COOH,[29] suggesting enhanced interactions within the system.[30] Overall, the

https://doi.org/10.1021/acsomega.3c10135
ACS Omega 2024, 9, 49001−49012

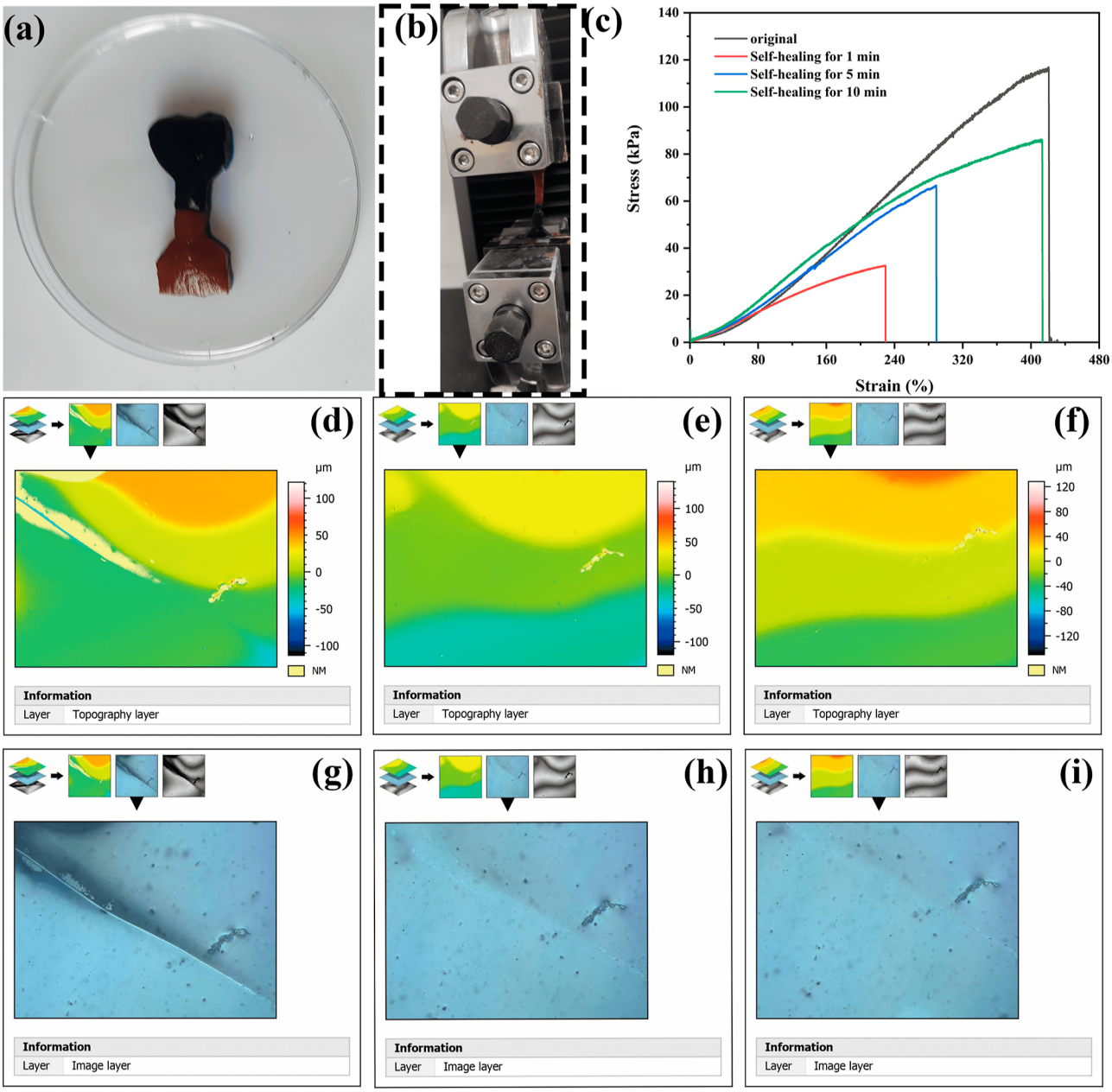

Figure 3. (a) Image of the P_{Ag}CHB hydrogel stained with rhodamine 6G and methyl blue. (b) Stretching process of the healed P_{Ag}CHB hydrogel. (c) Stress−strain curves of the P_{Ag}CHB hydrogel with different times of healing. Topography of the P_{Ag}CHB hydrogel healing for (d) 10, (e) 20, and (f) 30 s. Optical images of the P_{Ag}CHB hydrogel healing for (g) 10, (h) 20, and (i) 30 s.

composite hydrogel network of P_{Ag}HCB is primarily constructed through borate ester bonds between *cis*-diol sites of PVA chains and borax. Additionally, it is complemented by hydrogen bonds among PVA, HPMC, AgNPs, and CNT-COOH (Figure 1b).

Typically, the primary structural decomposition temperature of PVA hydrogels is around 275 °C.[31] However, for silver nanohydrogels cross-linked with borax, the primary structural decomposition temperature is approximately 290 °C. This suggests that the chemical cross-linking significantly enhances thermal stability, primarily due to the formation of borate bonds, even though silver nitrate oxidizes some hydroxyl groups on the molecular chains of PVA. With the incorporation of HPMC and CNT-COOH, there is a noticeable increase in the solid residue of the gel after thermogravimetric testing (Figure S2a). The hydrogel with added HPMC exhibits a higher decomposition temperature, increasing from 297.7 to 307.6 °C, indicating a stronger interaction between the PVA and HPMC molecular chains, resulting in the formation of denser hydrogen bonds.[32] This interaction is manifested in the changes in the peak width at 3300 cm^{-1} and the shift in maximum absorption wavelengths in the infrared spectra. Importantly, the maximum decomposition rate of the gel, corresponding to the decomposition temperature, increased from 307.6 to 313.6 °C after the addition of CNT-COOH (Figure S2b), suggesting that the introduction of CNT-COOH led to more significant interactions between polymer chain segments within the hydrogel.[33]

https://doi.org/10.1021/acsomega.3c10135
ACS Omega 2024, 9, 49001−49012

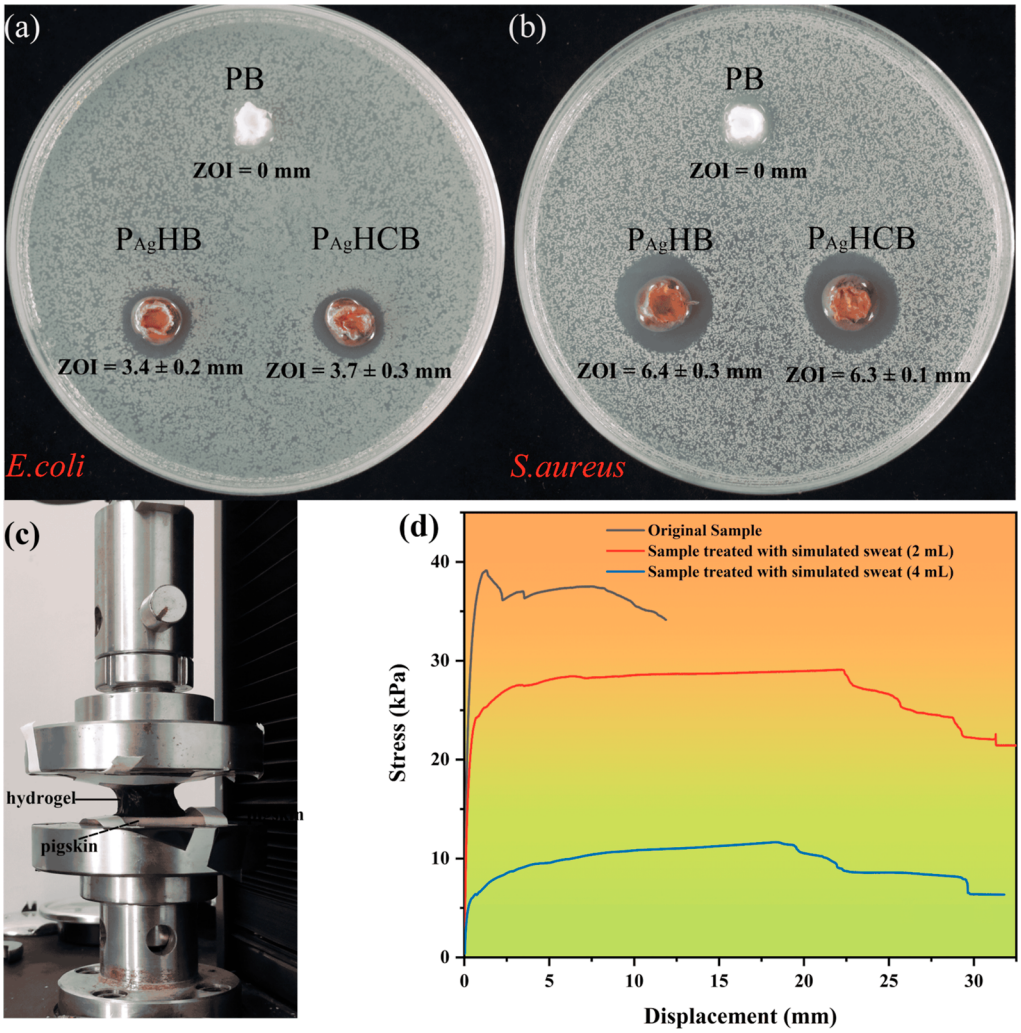

Figure 4. Antimicrobial properties of PB, P_{Ag}HB, and P_{Ag}HCB hydrogels against (a)*E. coli* and (b) *S. aureus*. (c) Adhesion testing procedure of the P_{Ag}HCB hydrogel on pig skin. (d) Adhesion strength of the P_{Ag}HCB hydrogel on pig skins treated by simulated sweat.

Characterization of Mechanical and Self-Healing Properties of P_{Ag}HCB Hydrogels. A balance between the rigidity and toughness of the hydrogel was achieved by optimizing the mechanical properties of the hydrogel.[34] After the formation of nanosilver after UV irradiation, the mechanical properties (Figure 2g) of the prepared hydrogel P_{Ag}B were slightly reduced, which was attributed to the oxidation of the hydroxyl groups on the molecular chain of PVA by silver ions, resulting in a decrease in the hydrogen bonding density of the hydrogel. The introduction of HPMC and CNT-COOH significantly enhances the mechanical strength of the hydrogel, which compensates for the decrease in mechanical strength caused by oxidative reactions. From the intricate TEM diffraction patterns (Figure S6a), it is evident that the hydrogel contains various crystal structures, attributed to nanosilver, PVA crystalline regions, and other polymer crystallites. Transmission imaging (Figure S6b) reveals nanosilver particles enveloped by polymer chains, indicating the encapsulating effect of HPMC. Furthermore, X-ray diffraction (XRD) spectrum (Figure S6c) confirms the presence of nanosilver particles within the gel, while X-ray photoelectron spectroscopy (XPS) spectra (Figure S6d) indicate the valence states of silver elements inside the gel, including monovalent silver ions and zerovalent nanosilver particles. Integration of the diffraction peaks reveals an approximate content ratio of 3:2.

In addition, the strength of the hydrogel was significantly enhanced by the addition of HPMC, and the SEM images (Figure 2d–f) showed the formation of a denser pore structure, suggesting a stronger chemical bonding between the molecular chains of PVA and HPMC. The prepared hydrogels could be bent, twisted, and knotted without permanent deformation (Figure 2a–c). To ascertain the content of CNT-COOH, the tensile properties of the P_{Ag}HCB hydrogel were evaluated at various CNT-COOH concentrations, revealing that 10 mg/mL was the optimal choice (Figure 2h). From the cyclic tensile (Figure S7a) and compressive (Figure S7b) tests of the gel, it is observed that due to stress relaxation, the mechanical strength of the gel decreases in the first three cycles. However, in subsequent cycles, the mechanical performance tends to stabilize, indicating that the gel exhibits good mechanical recovery properties.

In order to evaluate the self-healing ability of these hydrogels, tensile tests (Figure 3b) were performed on the specimens after staining with rhodamine 6G and methyl blue (Figure 3a). The results showed that the hydrogels were able to achieve a healing efficiency of more than 70% after a 10 min

https://doi.org/10.1021/acsomega.3c10135
ACS Omega 2024, 9, 49001−49012

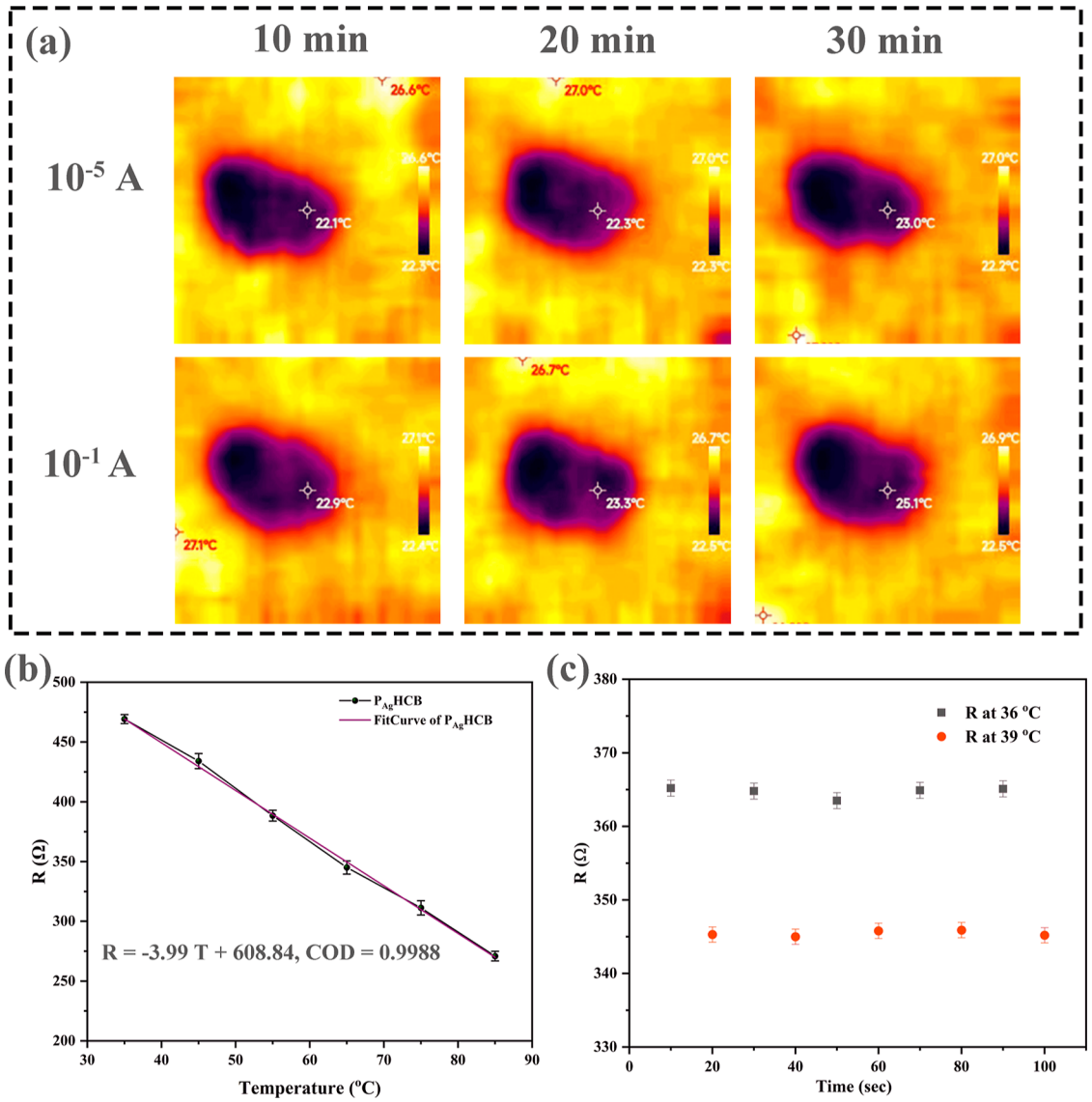

Figure 5. (a) Thermal imaging of surface on the P_{Ag}HCB hydrogel at different currents and energization times. (b) Resistance values of the P_{Ag}HCB hydrogel at different temperatures. (c) Resistance values of the P_{Ag}HCB hydrogel at normal body temperature (36 °C) and feverish body temperature (39 °C).

healing process (Figure 3c). In order to characterize the self-healing process more visually, the specimens were subjected to laser confocal microscopy.[35] The reparative dynamics of the P_{Ag}HCB hydrogel and the surface irregularities of the fractured area can be observed through topographic mapping (Figure 3d–f) at intervals of 10, 20, and 30 s during the healing process. After a duration of 30 s, hydrogel fracture exhibits a nearly complete self-healing state (Figure 3g–i).

Electrical Properties of the P_{Ag}HCB Hydrogel. The silver nanoparticles within the P_{Ag}HCB hydrogel created ionic conductive conditions for ion transport, and CNT-COOH increased the conductive pathways within the hydrogel, significantly improving their electrical conductivity.[36] To ensure the electrical stability of the hydrogel during the testing period, we monitored the rate of change in its electrical resistance in air. The experimental results showed that the conductivity of P_{Ag}B, P_{Ag}HB, and P_{Ag}HCB hydrogels slightly increased during the first 2 h of exposure to air, which was due to the decrease in moisture content and the densification of the internal conductive pathways, whereas, with the extension of time, the conductivity of P_{Ag}B hydrogels decreased significantly, which was caused by the aggregation and oxidation of silver nanoparticles. In contrast, the conductivities of P_{Ag}HB and P_{Ag}HCB hydrogels decreased slightly, and the conductivity of the P_{Ag}HCB hydrogel was the most stable (Figure S4). Additionally, dynamic light scattering testing revealed that the size of silver nanoparticles within the hydrogel became more uniform after the addition of HPMC (Figure S5), with a slight increase in size.[37]

Antimicrobial and Adhesion Properties of the P_{Ag}HCB Hydrogel. The antimicrobial mechanism of nanosilver is mainly the disruption of cell membranes by silver ions and the effect on internal biochemical processes (DNA replication, etc.).[38−42] In order to assess the antimicrobial capacity of the hydrogel, we used the antimicrobial disk diffusion method to evaluate its effect on the growth of *S. aureus* and *E. coli*.

The results showed that no visible ZOI was found around the PB, indicating the poor antimicrobial performance of this sample. Although there were visible growth inhibition zones all

https://doi.org/10.1021/acsomega.3c10135
ACS Omega 2024, 9, 49001−49012

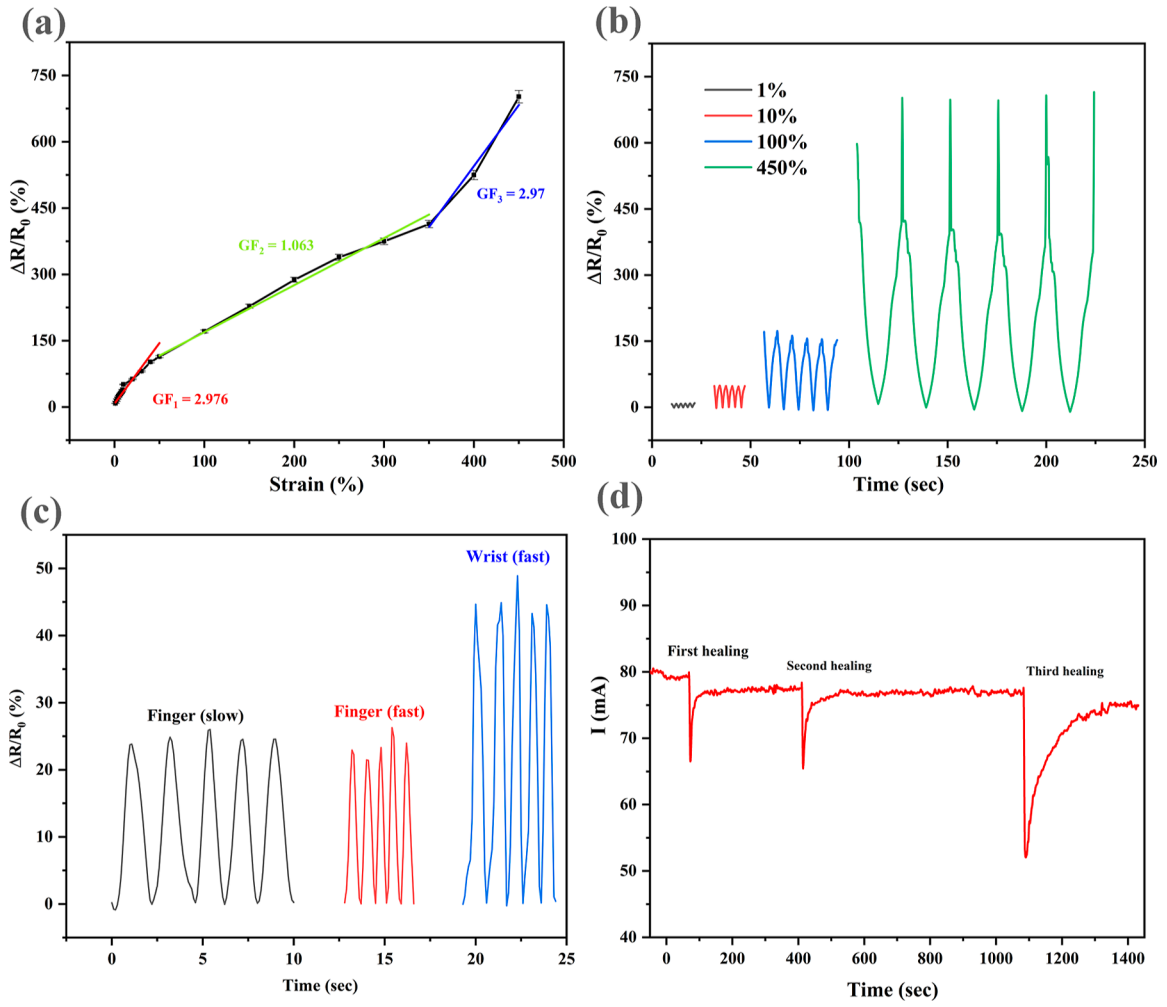

Figure 6. (a) Resistance variability of the P_{Ag}HCB hydrogel under different strains and their fitted curves. (b) Repeated sensing curves of the P_{Ag}HCB hydrogel at a strain of 1, 10, 100, and 450%. (c) P_{Ag}HCB hydrogel detects sensing signals from finger and wrist movements. (d) Electrical signals of the healing process of the P_{Ag}HCB hydrogel after three disruptions.

around P_{Ag}HB, the introduction of silver nanoparticles enabled the hydrogel to exhibit antimicrobial properties against both *E. coli* (ZOI = 3.4 ± 0.2 mm, Figure 4a) and *S. aureus* (ZOI = 6.4 ± 0.3 mm, Figure 4b). In addition, there was no significant difference in the size of the ZOI around P_{Ag}HCB compared to P_{Ag}HB. It suggests that although the introduction of CNT-COOH led to the enhancement of the interaction of the hydrogel, the release of silver ions inside them was not weakened.

In the adhesion experiment, it can be seen that the hydrogel adheres tightly to the surface of the pig skin (Figure 4c), and its adhesion strength in the dry state can be obtained through the tensile experiment. After the simulated sweat treatment, the adhesion strength of the hydrogel on the pig skin gradually decreased with the increase in the volume of simulated sweat. However, the adhesion strength of the hydrogel still remained above 10 kPa when 4 mL of simulated sweat was used (Figure 4d) and did not fall off from the pig skin, which indicated that the hydrogel was suitable for use as an epidermal sensor.[43,44] This stronger tissue adhesion property is generated as follows: the hydroxyl groups in the cross-linked network of PVA make it more hydrophilic, which helps the hydrogel form a stronger adhesion with the surface of biological tissues. Hydroxyl groups and the surface of biological tissues may undergo hydrogen bonding or other interactions that contribute to the strong adhesion of the hydrogel to the tissue surface. The hydroxyl and methyl groups in the molecular structure of HPMC are able to interact with the surface of biological tissues and increase the hydrogel's affinity for the surface. The adhesion mechanism of the hydrogel is illustrated in Figure S8. In summary, a large number of hydroxyl groups and silver ions in the gel form numerous hydrogen bonds, coordination, and electrostatic interactions with human skin. Additionally, experiments were conducted to assess adhesion to different material surfaces (Figure S9). The gel exhibited good adhesion to metal surfaces such as copper and steel plates, rubber plates, and glass plates, with the highest adhesion strength observed on rubber plates.

Temperature Response Properties of P_{Ag}HCB Hydrogels. The hydrogel composed of borate ester bonds exhibits temperature sensitivity.[45−47] Initially, a change in the coordination state of the borate ester bonds occurs with a temperature variation, leading to the dissociation of these bonds. Consequently, the cross-linking density of the hydrogel decreases, resulting in an increase in the conductivity of the gel as the internal conducting pathways become more pronounced.[48,49]

https://doi.org/10.1021/acsomega.3c10135
ACS Omega 2024, 9, 49001−49012

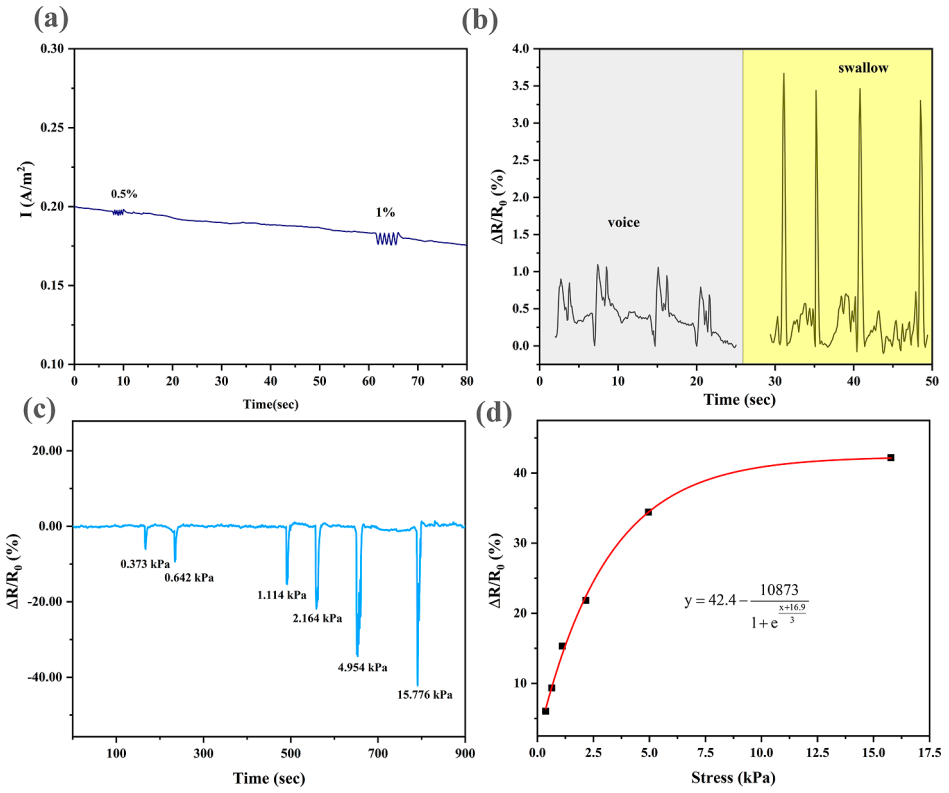

Figure 7. (a) Electrical signals of the P_{Ag}HCB hydrogel under small deformations. (b) Sensing electrical signals from the P_{Ag}HCB hydrogel for speaking and swallowing processes. (c) Resistance variability of the P_{Ag}HCB hydrogel pressure sensor with different compressive stress. (d) Scatter plot upon the change rate of resistance of the P_{Ag}HCB hydrogel pressure sensor at different stress and the fitted curve.

Furthermore, the temperature-induced alteration in the coordination state of borate ester bonds facilitates their dissociation, contributing to a reduction in the cross-linking density within the hydrogel.[50−52] This, in turn, enhances the internal conductivity pathways, leading to an elevation in electrical conductivity.[53,54] Additionally, the temperature-dependent migration rate of ions within the gel increases, further augmenting the gel's electrical conductivity. To investigate the temperature responsiveness of the P_{Ag}HCB hydrogel, it is first necessary to exclude the Joule effect caused by electrical energization. As shown in the figure, the surface temperature of the gel only slightly changes when a current of 0.1 A is applied for 30 min (Figure 5a), whereas there is no significant temperature change on the surfaces of other samples. Additionally, the working current of the electrochemical workstation is generally around 10^{-3} A. Therefore, utilizing the electrochemical workstation for characterizing the temperature sensitivity of the gel can neglect the Joule effect.

Next, the gel was heated by using a heating table, and the resistance values of the gel at 30, 40, 50, 60, 70, and 80 °C were determined. After linear fitting, it was observed that the resistivity of the P_{Ag}HCB hydrogel is linearly correlated with temperature, with the equation $R = -3.99T + 608.84$, where the COD (coefficient of determination) is 0.9988 (Figure 5b). Based on the excellent linear temperature responsiveness, experiments were conducted to simulate the monitoring of human body temperature. By repeatedly measuring the resistance values of the gel at normal body temperature (36 °C) and feverish body temperature (39 °C) (Figure 5c), it was observed that the approximate judgment of human body temperature could be made by observing the resistance values of the gel. This suggests the potential for real-time monitoring of human body temperature.[55−57]

Tensile and Pressure Sensors Prepared from the P_{Ag}HCB Hydrogel. The change in electrical resistance of the hydrogels during stretching was evaluated using an electrochemical workstation and a universal stretching machine. Scatter plots showed that the hydrogel exhibited three different linear sensing regions corresponding to different gauge factors (Figure 6a). The first segment reflected the change in electrical signals due to slight deformation with a gauge factor of 2.976. The second segment presented a stable sensing stage, during which the hydrogel could undergo repeated stretching sensing, benefiting from the gel's elastic recovery. The sudden increase in strain coefficient observed in the last segment was due to the disruption of the internal network structure of the gel as the strain continued to increase, resulting in the breakdown of the conductive pathways and a significant decrease in conductivity. However, due to the excellent healing ability of the hydrogel, this process could still be repeated many times.[58−60] As a result, repetitive electrical signals can be detected under different deformations (Figure 6b).The corresponding key performance parameters of gel sensors are compared with those in the literature, as shown in the following Table S2.

Strain sensors exhibited rapid and significant real-time changes in resistance in response to rapid movements in different joints such as the wrist and fingers. These findings suggest that hydrogel sensors have the potential to diagnose joint diseases and monitor motor behavior. Importantly, the peak signal width clearly differentiated the rate of finger flexion (Figure 6c). Furthermore, the sensor can perform motion detection on large joints, such as knee and elbow joints (Figure S10). By comparing the rate of resistance changes and the

https://doi.org/10.1021/acsomega.3c10135
ACS Omega 2024, 9, 49001−49012

shape of peaks, it can determine the body's movement status. Additionally, signals generated by each joint movement were highly similar, indicating that the hydrogel has outstanding recovery ability and sensitivity. Three disruption experiments were also conducted to test the electrical self-healing ability of the gel, and it was found that the gel still retained a high conductivity after three disruptions (Figure 6d). The gel sensor can detect stable real-time electrical signals under different strains (Figure S11a). The response time and release time of the sensor are 500 and 600 ms (Figure S11b), respectively.

Furthermore, strain sensors accurately detected changes in electrical signals caused by small deformations (Figure 7a,b) during human speech.[61,62]

In addition, a pressure sensor made of the P_{Ag}HCB hydrogel responded to different electrical signals for various pressure effects (Figure 7c). The following formula was obtained by fitting the rate of resistance change of the pressure sensor and compressive stress, indicating that the sensitivity of the sensor decreases with increasing strain in compression (Figure 7d). This is advantageous for the hydrogel in monitoring the signals of small deformations.

$$y = 42.4 - \frac{10873}{1 + e^{\frac{x+16.9}{3}}} \quad (3)$$

where y denotes the change rate of resistance of the pressure sensor and x denotes the stress applied to the sensor.

CONCLUSIONS

In conclusion, we have successfully prepared a hydrogel flexible sensor with conductive, fast self-healing, self-adhesive, and temperature-responsive properties. The hydrogel was prepared by a mild method in which dynamic covalent and hydrogen bonding interactions dominated, employing extremely biocompatible PVA and HPMC as the hydrogel network by slow cross-linking with borax, where CNT-COOH and nanosilver were used as conductive fillers and reinforcing fillers. With a rapid self-healing capability of approximately 30 s and an impressive healing efficiency of 74.1%, the hydrogel maintains robust adhesion even in conditions of sweaty skin. Moreover, it exhibits commendable antimicrobial properties, ensuring that the sensor−skin contact interface remains devoid of metabolic and biological contamination. The strain sensor constructed from the P_{Ag}HCB hydrogel has three different strain intervals, corresponding to three different strain factors, and is capable of monitoring the movements of human fingers, wrists, and other joints, as well as capturing electrical signals generated by small deformations such as speaking and swallowing. The pressure sensor constructed by P_{Ag}HCB has a high sensitivity for sensing and detecting small deformations. In addition, the sensor has a good linear temperature response for detecting changes in the body temperature. Overall, we believe that this work constructs multifunctional conductive hydrogel sensors, which makes the hydrogel suitable for a variety of complex application scenarios (temperature monitoring, motion monitoring, etc.) and contributes to the advancement of constructing multifunctional conductive hydrogel sensors.

ASSOCIATED CONTENT

Supporting Information

The Supporting Information is available free of charge at https://pubs.acs.org/doi/10.1021/acsomega.3c10135.

Infrared spectra of different components of hydrogels; TG and DTG curves of the P_{Ag}B, P_{Ag}HB, and P_{Ag}HCB hydrogels; three-dimensional drawing and physical photo of the mold; changes in the weight and conductivity of P_{Ag}B, P_{Ag}HB, and P_{Ag}HCB hydrogels after placing in air for different periods of time; particle size distributions of AgNPs within P_{Ag}B, P_{Ag}HB, and P_{Ag}HCB hydrogels; transmission diffraction pattern, transmission imaging, XRD pattern, and XPS spectrum of the P_{Ag}HCB hydrogel; stress−strain curves for cyclic tensile and cyclic compressive loading of the P_{Ag}HCB hydrogel; schematic representation of the adhesive properties, self-healing capabilities, and temperature-responsive behaviors of the P_{Ag}HCB hydrogel; adhesion states and adhesive strength of the P_{Ag}HCB hydrogel on surfaces of different materials; motion detection of the P_{Ag}HCB hydrogel sensor for knee and elbow joints; real-time electrical signal detection of the P_{Ag}HCB hydrogel sensor under various tensile strains and the response time and release time of the sensor; composition of the prepared hydrogels; and corresponding key performance parameters of gel sensors are compared with those in the literature (PDF)

AUTHOR INFORMATION

Corresponding Author

Xia Huang − *School of Materials Science and Engineering, Zhengzhou University, Zhengzhou, Henan 450001, P. R. China*; Email: happyhxia@163.com

Authors

Xiongbiao Zheng − *School of Materials Science and Engineering, Zhengzhou University, Zhengzhou, Henan 450001, P. R. China*; orcid.org/0000-0002-3177-1102

Jiachang Chen − *Henan Provincial Institute of Cultural Relics and Archaeology, Zhengzhou, Henan 450000, P. R. China*

Complete contact information is available at: https://pubs.acs.org/10.1021/acsomega.3c10135

Notes

The authors declare no competing financial interest.

ACKNOWLEDGMENTS

The author thanks all those who provided skills, resources, and advice for this study and whose contributions were essential for us to complete this work.

REFERENCES

(1) Wang, L.; Xu, T.; Zhang, X. Multifunctional conductive hydrogel-based flexible wearable sensors. *TrAC, Trends Anal. Chem.* **2021**, *134*, 116130.

(2) Sun, X.; Yao, F.; Li, J. Nanocomposite hydrogel-based strain and pressure sensors: a review. *J. Mater. Chem. A* **2020**, *8*, 18605−18623.

(3) Rahmani, P.; Shojaei, A. A review on the features, performance and potential applications of hydrogel-based wearable strain/pressure sensors. *Adv. Colloid Interface Sci.* **2021**, *298*, 102553.

(4) Li, S.; Cong, Y.; Fu, J. Tissue adhesive hydrogel bioelectronics. *J. Mater. Chem. B* **2021**, *9*, 4423−4443.

(5) Lee, H. R.; Kim, C. C.; Sun, J. Y. Stretchable Ionics - A Promising Candidate for Upcoming Wearable Devices. *Adv. Mater.* **2018**, *30*, No. e1704403.

(6) Chen, Z.; Chen, Y.; Hedenqvist, M. S.; Chen, C.; Cai, C.; Li, H.; Liu, H.; Fu, J. Multifunctional conductive hydrogels and their

applications as smart wearable devices. *J. Mater. Chem. B* **2021**, *9*, 2561−2583.
(7) Yang, T.; Xu, C.; Liu, C.; Ye, Y.; Sun, Z.; Wang, B.; Luo, Z. Conductive polymer hydrogels crosslinked by electrostatic interaction with PEDOT:PSS dopant for bioelectronics application. *Chem. Eng. J.* **2022**, *429*, 132430.
(8) Wang, T.; Farajollahi, M.; Henke, S.; Zhu, T.; Bajpe, S. R.; Sun, S.; Barnard, J. S.; Lee, J. S.; Madden, J. D. W.; Cheetham, A. K.; Smoukov, S. K. Functional conductive nanomaterials via polymerisation in nano-channels: PEDOT in a MOF. *Mater. Horiz.* **2017**, *4*, 64−71.
(9) Yang, M.; Ren, X.; Yang, T.; Xu, C.; Ye, Y.; Sun, Z.; Kong, L.; Wang, B.; Luo, Z. Polypyrrole/sulfonated multi-walled carbon nanotubes conductive hydrogel for electrochemical sensing of living cells. *Chem. Eng. J.* **2021**, *418*, 129483.
(10) Huang, J.; Huang, X.; Wu, P. One stone for three birds: One-step engineering highly elastic and conductive hydrogel electronics with multilayer MXene as initiator, crosslinker and conductive filler simultaneously. *Chem. Eng. J.* **2022**, *428*, 132515.
(11) Xu, Y.; Rothe, R.; Voigt, D.; Hauser, S.; Cui, M.; Miyagawa, T.; Patino Gaillez, M.; Kurth, T.; Bornhauser, M.; Pietzsch, J.; Zhang, Y. Convergent synthesis of diversified reversible network leads to liquid metal-containing conductive hydrogel adhesives. *Nat. Commun.* **2021**, *12*, 2407.
(12) Srikhao, N.; Theerakulpisut, S.; Chindaprasirt, P.; Okhawilai, M.; Narain, R.; Kasemsiri, P. Green synthesis of nano silver-embedded carboxymethyl starch waste/poly vinyl alcohol hydrogel with photothermal sterilization and pH-responsive behavior. *Int. J. Biol. Macromol.* **2023**, *242*, 125118.
(13) Yang, P.; Li, Z.; Fang, B.; Liu, L. Self-healing hydrogels based on biological macromolecules in wound healing: A review. *Int. J. Biol. Macromol.* **2023**, *253*, 127612.
(14) Zhao, L.; Ren, Z.; Liu, X.; Ling, Q.; Li, Z.; Gu, H. A Multifunctional, Self-Healing, Self-Adhesive, and Conductive Sodium Alginate/Poly(vinyl alcohol) Composite Hydrogel as a Flexible Strain Sensor. *ACS Appl. Mater. Interfaces* **2021**, *13*, 11344−11355.
(15) Adelnia, H.; Ensandoost, R.; Shebbrin Moonshi, S.; Gavgani, J. N.; Vasafi, E. I.; Ta, H. T. Freeze/thawed polyvinyl alcohol hydrogels: Present, past and future. *Eur. Polym. J.* **2022**, *164*, 110974.
(16) Cromwell, O. R.; Chung, J.; Guan, Z. Malleable and Self-Healing Covalent Polymer Networks through Tunable Dynamic Boronic Ester Bonds. *J. Am. Chem. Soc.* **2015**, *137*, 6492−6495.
(17) Alavi, M.; Ashengroph, M. Mycosynthesis of AgNPs: mechanisms of nanoparticle formation and antimicrobial activities. *Expert Rev. Anti-infective Ther.* **2023**, *21*, 355−363.
(18) Taesuwan, I.; Ounkaew, A.; Okhawilai, M.; Hiziroglu, S.; Jarernboon, W.; Chindaprasirt, P.; Kasemsiri, P. Smart conductive nanocomposite hydrogel containing green synthesized nanosilver for use in an eco-friendly strain sensor. *Cellulose* **2022**, *29*, 273−286.
(19) Singh, A.; Sharma, J. J.; Mohanta, B.; Sood, A.; Han, S. S.; Sharma, A. Synthetic and biopolymers-based antimicrobial hybrid hydrogels: a focused review. *J. Biomater. Sci., Polym. Ed.* **2024**, *35*, 675−716.
(20) Abe, S.; Nesabi, M.; Safaee, S.; Seitoku, E.; Yato, Y.; Hyono, A.; Era, Y.; Nakanishi, K.; Nakamura, M.; Kusaka, T.; Valanezhad, A.; Takada, T.; Watanabe, I. A novel thermoresponsive hydrogel composite controlled by infrared irradiation. *Mol. Cryst. Liq. Cryst.* **2023**, *763*, 73−79.
(21) Tu, H.; Zhou, M.; Yi, R.; Gu, Y.; Bu, J. Preparation and characterisation of a high-strength self-healing hydrogel. *Plast., Rubber Compos.* **2021**, *50*, 1−8.
(22) Shamshuddin, M. D.; Salawu, S. O.; Bég, O. A.; Kadir, A.; Bég, T. A. Computation of reactive mixed convection radiative viscoelastic nanofluid thermo-solutal transport from a stretching sheet with Joule heating. *Int. J. Model. Simulat.* **2022**, *42*, 1005−1029.
(23) Liu, R.; Li, Y.; Chen, J.; Zhang, X.; Niu, Z.; Sun, Y. The preparation of multifunction chitosan adhesive hydrogel by "one-step" method. *J. Biomater. Sci., Polym. Ed.* **2020**, *31*, 1925−1940.
(24) Gu, Y.; Miao, F.; Liu, K.; Su, Y.; Wei, Y.; Hu, Y.; Lian, X.; Han, W.; Chen, W.; Huang, D. Fabrication of gelatin methacryloyl/graphene oxide conductive hydrogel for bone repair. *J. Biomater. Sci., Polym. Ed.* **2023**, *34*, 2076−2090.
(25) Wang, T.; Zhang, F.; Zhao, R.; Wang, C.; Hu, K.; Sun, Y.; Politis, C.; Shavandi, A.; Nie, L. Polyvinyl Alcohol/Sodium Alginate Hydrogels Incorporated with Silver Nanoclusters via Green Tea Extract for Antibacterial Applications. *Des. Monomers Polym.* **2020**, *23*, 118−133.
(26) Varshney, S.; Maurya, A. K.; Kanaujia, A.; Mishra, N. Silica from waste rice husk and its polymeric hydrogel-based composite filler: synthesis, characterisation, and antibacterial activity. *Adv. Mater. Process. Technol.* **2023**, 1−16.
(27) Khan, S.; Minhas, M. U.; Ahmad, M.; Sohail, M. Self-assembled supramolecular thermoreversible β-cyclodextrin/ethylene glycol injectable hydrogels with difunctional Pluronic 127 as controlled delivery depot of curcumin. Development, characterization and *in vitro* evaluation. *J. Biomater. Sci., Polym. Ed.* **2018**, *29*, 1−34.
(28) Song, B.; Ren, Z.; Gu, H. Totally dynamically cross-linked dual-network conductive hydrogel with superb and rapid self-healing ability for motion detection sensors. *Mater. Today Commun.* **2023**, *35*, 105919.
(29) Fan, X.; Zhao, L.; Ling, Q.; Liu, J.; Gu, H. Mussel-induced nano-silver antibacterial, self-healing, self-adhesive, anti-freezing, and moisturizing dual-network organohydrogel based on SA-PBA/PVA/CNTs as flexible wearable strain sensors. *Polymer* **2022**, *256*, 125270.
(30) Zhang, C.-H.; Luo, Y.-L.; Chen, Y.-S.; Wei, Q.-B.; Fan, L.-H. Preparation and Theophylline Delivery Applications of Novel PMAA/MWCNT-COOH Nanohybrid Hydrogels. *J. Biomater. Sci., Polym. Ed.* **2009**, *20*, 1119−1135.
(31) Luo, X.; Zhu, L.; Wang, Y.-C.; Li, J.; Nie, J.; Wang, Z. L. A Flexible Multifunctional Triboelectric Nanogenerator Based on MXene/PVA Hydrogel. *Adv. Funct. Mater.* **2021**, *31*, 2104928.
(32) Weiss, P.; Vinatier, C.; Sohier, J.; Fatimi, A.; Layrolle, P.; Demais, V.; Atmani, H.; Basle, M.-F.; Guicheux, J. Self-Hardening Hydrogel for Bone Tissue Engineering. *Macromol. Symp.* **2008**, *266*, 30−35.
(33) Hashmi, S.; Nadeem, S.; García-Peñas, A.; Ahmed, R.; Zahoor, A.; Vatankhah-Varnoosfaderani, M.; Stadler, F. J. Study the Effects of Supramolecular Interaction on Diffusion Kinetics in Hybrid Hydrogels of Zwitterionic Polymers and CNTs. *Macromol. Chem. Phys.* **2022**, *223*, 2100348.
(34) Zhou, S.; Guo, K.; Bukhvalov, D.; Zhang, X.-F.; Zhu, W.; Yao, J.; He, M. Cellulose Hydrogels by Reversible Ion-Exchange as Flexible Pressure Sensors. *Adv. Mater. Technol.* **2020**, *5*, 2000358.
(35) Paterson, S. M.; Casadio, Y. S.; Brown, D. H.; Shaw, J. A.; Chirila, T. V.; Baker, M. V. Laser scanning confocal microscopy versus scanning electron microscopy for characterization of polymer morphology: Sample preparation drastically distorts morphologies of poly(2-hydroxyethyl methacrylate)-based hydrogels. *J. Appl. Polym. Sci.* **2013**, *127*, 4296−4304.
(36) Yu, Y.; Feng, Y.; Liu, F.; Wang, H.; Yu, H.; Dai, K.; Zheng, G.; Feng, W. Carbon Dots-Based Ultrastretchable and Conductive Hydrogels for High-Performance Tactile Sensors and Self-Powered Electronic Skin. *Small* **2023**, *19*, 2204365.
(37) Talodthaisong, C.; Patramanon, R.; Thammawithan, S.; Lapmanee, S.; Maikaeo, L.; Sricharoen, P.; Khongkow, M.; Namdee, K.; Jantimaporn, A.; Kayunkid, N.; Hutchison, J. A.; Kulchat, S. A Shear-Thinning, Self-Healing, Dual-Cross Linked Hydrogel Based on Gelatin/Vanillin/Fe3+/AGP-AgNPs: Synthesis, Antibacterial, and Wound-Healing Assessment. *Macromol. Biosci.* **2023**, *23*, 2300250.
(38) Zhang, H.; Wu, Z.; Zhou, J.; Wang, Z.; Yang, C.; Wang, P.; Fareed, M. S.; He, Y.; Su, J.; Cha, R.; Wang, K. The Antimicrobial, Hemostatic, and Anti-Adhesion Effects of a Peptide Hydrogel Constructed by the All-d-Enantiomer of Antimicrobial Peptide Jelleine-1. *Adv. Healthcare Mater.* **2023**, *12*, 2301612.
(39) Kundu, R.; Payal, P. Antimicrobial Hydrogels: Promising Soft Biomaterials. *ChemistrySelect* **2020**, *5*, 14800−14810.

https://doi.org/10.1021/acsomega.3c10135
ACS Omega 2024, 9, 49001−49012

(40) Jodar, K. S. P.; Balcao, V. M.; Chaud, M. V.; Tubino, M.; Yoshida, V. M. H.; Oliveira, J. M.; Vila, M. M. D. C. Development and Characterization of a Hydrogel Containing Silver Sulfadiazine for Antimicrobial Topical Applications. *J. Pharm. Sci.* **2015**, *104*, 2241−2254.
(41) Dey, R.; Mukherjee, R.; Haldar, J. Photo-Crosslinked Antimicrobial Hydrogel Exhibiting Wound Healing Ability and Curing Infections In Vivo. *Adv. Healthcare Mater.* **2022**, *11*, 2200536.
(42) An, H.; Yang, Y.; Bo, Y.; Ma, X.; Wang, Y.; Liu, L.; Wang, H.; He, Y.; Qin, J. Fabrication of self-healing hydrogel from quaternized N-[3(dimethylamino)propyl]methacrylamide copolymer for antimicrobial and drug release applications. *J. Biomed. Mater. Res., Part A* **2021**, *109*, 42−53.
(43) Yang, Z.; He, Y.; Ma, Y.; Li, L.; Wang, Y. A Reversible Adhesive Hydrogel Tape. *Adv. Funct. Mater.* **2023**, *33*, 2213150.
(44) Xu, R.; Lai, Y.; Liu, J.; Wei, Q.; Sheng, W.; Ma, S.; Lei, Z.; Zhou, F. A Strong and Double-sided Self-Adhesive Hydrogel Sensor. *Macromol. Rapid Commun.* **2023**, *44*, 2300182.
(45) Liu, P.; Zhang, S.; Wei, F.; Lv, J.; Xu, P. Synthesis and properties of elevated temperature hydrogels for enhanced oil recovery based on AM/AMPA/NVP copolymer and silica nanoparticles. *J. Appl. Polym. Sci.* **2023**, *140*, No. e54583.
(46) Zhang, R.; Bowyer, A.; Eisenthal, R.; Hubble, J. Temperature responsive pore-filled membranes based on a BSA/poly(N-isopropylacrylamide) hydrogel. *Adv. Polym. Technol.* **2008**, *27*, 27−34.
(47) Park, T. G.; Hoffman, A. S. Synthesis and characterization of pH- and/or temperature-sensitive hydrogels. *J. Appl. Polym. Sci.* **1992**, *46*, 659−671.
(48) He, W.; Xu, F.; Lu, S.; Zhang, Y.; Fan, H. Flexible and recoverable ion-conductive hydrogels with cross-linked triple network for highly sensitive wearable Motion-monitoring sensors. *Next Mater.* **2023**, *1*, 100027.
(49) Ghosh, S.; Majhi, J.; Sharma, S.; Priya, K.; Bandyopadhyay, A. A review on the development of electron and ion conductive polymer hydrogels and their composites for flexible and smart supercapacitors. *J. Energy Storage* **2023**, *74*, 109423.
(50) Gao, Z.; Zheng, G.; Yang, Y.; Zheng, D.; Zhou, X.; Xu, Y.; Zeng, B.; Luo, W.; Chen, G.; Yuan, C.; Dai, L. Electrically controlled underwater object manipulation with adhesive borate ester hydrogels. *Mater. Today Nano* **2023**, *24*, 100396.
(51) Cheng, H.; Fan, Z.; Wang, Z.; Guo, Z.; Jiang, J.; Xie, Y. Highly stretchable, fast self-healing nanocellulose hydrogel combining borate ester bonds and acylhydrazone bonds. *Int. J. Biol. Macromol.* **2023**, *245*, 125471.
(52) Liu, Y.; Chang, J.; Mao, J.; Wang, S.; Guo, Z.; Hu, Y. Dual-network hydrogels based on dynamic imine and borate ester bonds with antibacterial and self-healing properties. *Colloids Surf., B* **2023**, *230*, 113528.
(53) Zhang, Q.; Liu, X.; Duan, L.; Gao, G. Ultra-stretchable wearable strain sensors based on skin-inspired adhesive, tough and conductive hydrogels. *Chem. Eng. J.* **2019**, *365*, 10−19.
(54) Zhou, Y.; Wan, C.; Yang, Y.; Yang, H.; Wang, S.; Dai, Z.; Ji, K.; Jiang, H.; Chen, X.; Long, Y. Highly Stretchable, Elastic, and Ionic Conductive Hydrogel for Artificial Soft Electronics. *Adv. Funct. Mater.* **2019**, *29*, 1806220.
(55) Peng, X.; Wang, W.; Yang, W.; Chen, J.; Peng, Q.; Wang, T.; Yang, D.; Wang, J.; Zhang, H.; Zeng, H. Stretchable, compressible, and conductive hydrogel for sensitive wearable soft sensors. *J. Colloid Interface Sci.* **2022**, *618*, 111−120.
(56) Wang, Z.; Cong, Y.; Fu, J. Stretchable and tough conductive hydrogels for flexible pressure and strain sensors. *J. Mater. Chem. B* **2020**, *8*, 3437−3459.
(57) Rong, Q.; Lei, W.; Liu, M. Conductive Hydrogels as Smart Materials for Flexible Electronic Devices. *Chem.—Eur. J.* **2018**, *24*, 16930−16943.
(58) Li, S.; Cong, Y.; Fu, J. Tissue adhesive hydrogel bioelectronics. *J. Mater. Chem. B* **2021**, *9*, 4423−4443.
(59) He, P.; Guo, R.; Hu, K.; Liu, K.; Lin, S.; Wu, H.; Huang, L.; Chen, L.; Ni, Y. Tough and super-stretchable conductive double network hydrogels with multiple sensations and moisture-electric generation. *Chem. Eng. J.* **2021**, *414*, 128726.
(60) Han, S.; Liu, C.; Lin, X.; Zheng, J.; Wu, J.; Liu, C. Dual Conductive Network Hydrogel for a Highly Conductive, Self-Healing, Anti-Freezing, and Non-Drying Strain Sensor. *ACS Appl. Polym. Mater.* **2020**, *2*, 996−1005.
(61) Han, L.; Yan, L.; Wang, M.; Wang, K.; Fang, L.; Zhou, J.; Fang, J.; Ren, F.; Lu, X. Transparent, Adhesive, and Conductive Hydrogel for Soft Bioelectronics Based on Light-Transmitting Polydopamine-Doped Polypyrrole Nanofibrils. *Chem. Mater.* **2018**, *30*, 5561−5572.
(62) Han, L.; Lu, X.; Wang, M.; Gan, D.; Deng, W.; Wang, K.; Fang, L.; Liu, K.; Chan, C. W.; Tang, Y.; Weng, L.-T.; Yuan, H. A Mussel-Inspired Conductive, Self-Adhesive, and Self-Healable Tough Hydrogel as Cell Stimulators and Implantable Bioelectronics. *Small* **2017**, *13*, 1601916.

https://doi.org/10.1021/acsomega.3c10135
ACS Omega 2024, 9, 49001−49012